Available online at www.sciencedirect.com
SCIENCE DIRECT®
Physics of the Earth and Planetary Interiors 152 (2005) 22–42
PHYSICS OF THE EARTH AND PLANETARY INTERIORS
www.elsevier.com/locate/pepi

Numerical models of the Earth's thermal history: Effects of inner-core solidification and core potassium

S.L. Butler[a,*], W.R. Peltier[b], S.O. Costin[a]

[a] *Department of Geological Sciences, University of Saskatchewan, 114 Science Place, Saskatoon, Sask., Canada S7N 5E2*
[b] *Department of Physics, University of Toronto, 60 St. George, Toronto, Ont., Canada M5S 1A7*

Received 8 October 2004; received in revised form 28 March 2005; accepted 20 May 2005

Abstract

Recently there has been renewed interest in the evolution of the inner core and in the possibility that radioactive potassium might be found in significant quantities in the core. The arguments for core potassium come from considerations of the age of the inner core and the energy required to sustain the geodynamo [Nimmo, F., Price, G.D., Brodholt, J., Gubbins, D., 2004. The influence of potassium on core and geodynamo evolution. Geophys. J. Int. 156, 363–376; Labrosse, S., Poirier, J.-P., Le Mouël, J.-L., 2001. The age of the inner core. Earth Planet Sci. Lett. 190, 111–123; Labrosse, S., 2003. Thermal and magnetic evolution of the Earth's core. Phys. Earth Planet Int. 140, 127–143; Buffett, B.A., 2003. The thermal state of Earth's core. Science 299, 1675–1677] and from new high pressure physics analyses [Lee, K., Jeanloz, R., 2003. High-pressure alloying of potassium and iron: radioactivity in the Earth's core? Geophys. Res. Lett. 30 (23); Murthy, V.M., van Westrenen, W., Fei, Y.W., 2003. Experimental evidence that potassium is a substantial radioactive heat source in planetary cores. Nature 423, 163–165; Gessmann, C.K., Wood, B.J., 2002. Potassium in the Earth's core? Earth Planet Sci. Lett. 200, 63–78]. The Earth's core is also located at the lower boundary of the convecting mantle and the presence of radioactive heat sources in the core will affect the flux of heat between these two regions and will, as a result, have a significant impact on the Earth's thermal history. In this paper, we present Earth thermal history simulations in which we calculate fluid flow in a spherical shell representing the mantle, coupled with a core of a given heat capacity with varying degrees of internal heating in the form of ^{40}K and varying initial core temperatures. The mantle model includes the effects of the temperature dependence of viscosity, decaying radioactive heat sources, and mantle phase transitions. The core model includes the thermal effects of inner core solidification and we present models for which the final size of the inner core is the same that for the present-day Earth. We compare the results of simulations with and without the effects of inner core solidification and we compare the results of the numerical model with those of a parameterized model. Models with concentrations of potassium in the core of roughly 600 ppm best satisfy the present-day surface heat flow constraint; however, the core temperatures in these models are somewhat high. In addition, we find that models with lesser degrees of heating in the core can also satisfy the surface heat flow constraint provided that the mantle is in a particularly active state. Our models predict a relatively young inner core with the greatest age being 1756 Ma. We demonstrate that models with high core temperatures

* Corresponding author. Tel.: +1 306 966 5702; fax: +1 306 966 8593.
E-mail address: sam.butler@usask.ca (S.L. Butler).

0031-9201/$ – see front matter
doi:10.1016/j.pepi.2005.05.005

in the latter part of simulations result in high CMB heat flows which lead to predictions of young inner cores. For fixed initial core temperatures, this leads to a slight decrease in the predicted age of the inner core with increasing concentration of radioactive elements in the core.

Keywords: Thermal history; Numerical models; Inner-core growth; Potassium in the core

1. Introduction

The question as to whether radioactive potassium is present in significant quantities in the Earth's outer core is an important one as it has consequences for our understanding of the Earth's thermal evolution, the generation of the Earth's magnetic field through the geodynamo, and for the growth rate of the inner core. The concentration of potassium in bulk silicate Earth models is significantly lower than the concentration in C1 chondrites (e.g., Hart and Zindler, 1986; Lassiter, 2004). It is generally assumed that much of the Earth's potassium, it being a volatile element, was evaporated and lost to space during the early hot stages of the Earth's evolution (e.g., McDonough and Sun, 1995). If potassium can alloy with iron under core conditions, it is possible that some of the Earth's complement of potassium was instead sequestered into the core. In contrast with earlier studies (e.g., Chabot and Drake, 1999; Ito et al., 1993; Sherman, 1990), the recent high-pressure analyses of Murthy et al. (2003), Lee and Jeanloz (2003) and Gessmann and Wood (2002) indicate that potassium may alloy with iron under the conditions existing at the time of the formation of the Earth's core. However, the conditions required for potassium dissolution in a metallic alloy and the predicted concentration of potassium in the core vary significantly between studies and some recent studies continue to argue that high concentrations of potassium in the core are unlikely (e.g., McDonough, 2004).

Investigations of the Earth's thermal history have largely been carried out using parameterized models of convection in the Earth's mantle, the earliest of these analyses being those of Sharpe and Peltier (1978), Schubert et al. (1980) and Davies (1980). These studies indicated that, due to the strong relationship between mantle temperature and viscosity and hence convective heat transport efficiency, most of the heat flow measured at the Earth's surface today must be balanced by modern-day radioactive heat inputs into the mantle. Hence, the Urey ratio (the ratio of the internal heating rate to the surface heat flow) was found to be quite high and of the order of 0.8. However, geochemical models of the abundances of radioactive elements in the bulk silicate earth (e.g., Hart and Zindler, 1986) indicate a relatively low degree of internal heating in the mantle and a modern-day Urey ratio of roughly 0.4. The presence of radioactive heat sources in the Earth's core would allow for a greater flux of heat across the core-mantle boundary and might reconcile these diverging points of view. Breuer and Spohn (1993) considered this possibility using parameterized convection simulations. Their results indicate that such a reconciliation is possible if 1–2 silicate Earth budgets of potassium (corresponding to 3–6 TW of modern-day internal heating) were included in the core. We reconsider this scenario using a detailed numerical model of convection in the Earth's mantle to calculate the Earth's thermal evolution. An alternative solution to "the Urey ratio paradox" has been proposed by Butler and Peltier (2002) who demonstrated that this issue could also be resolved by incorporating the influence of time-dependent layering of the mantle general circulation caused by the Rayleigh number dependent effectiveness of the 660-km depth phase transformation in inhibiting radial mass flux.

The thermal effects of inner-core growth have been included previously in the parameterized thermal history models of Mollett (1984), Breuer and Spohn (1993), Nimmo et al. (2004) and have been included in numerical models of the Earth's evolution by Nakagawa and Tackley (2004). The total energy associated with the solidification of the inner core is roughly two orders of magnitude smaller than the total energy associated with radioactive decay in the mantle over the history of the Earth and is also much smaller than estimates of the energy due to core accretion and of the accretion of the planet (e.g., Stacey and Stacey, 1999). As a result, the effects of inner core solidification on the thermal history of the planet as a whole are quite

modest but the consequences for the thermal state of the core and for the generation of the Earth's magnetic field may be significant.

There have been some previous investigations of the Earth's thermal history using numerical mantle convection models with varying core temperatures and decaying internal heat sources. Arkani-Hamed et al. (1981) performed some early, low resolution simulations. Yuen et al. (1995) found that mantle avalanche events (e.g., Solheim and Peltier, 1994a) become more pronounced when time-dependent thermal boundary conditions and internal heating rates are involved and Honda and Iwase (1996) compared the results of their numerical model with that of a parameterized model. Recently, Nakagawa and Tackley (2004) used a two-dimensional flow model in cylindrical geometry to investigate the Earth's thermal evolution when a second compositional component is present in the mantle. They concluded that models with significant compositional layering best satisfy the constraints imposed by the surface heat flow, the CMB heat flow and the size of the inner core. Parameterized convection models have been used to investigate the Earth's thermal history due to the computational efficiency that they afford. Given the extraordinary increase in computing power in recent years, simulations of the Earth's thermal history using two-dimensional numerical models have become feasible which allow the investigation of lateral and short-timescale variations in temperature and heat flow and a more complete description of mantle physical processes.

In contrast with suggestions based on geochemical constraints which predict that the inner core crystallization began prior to 3.5 Ga (Brandon et al., 2003), recent energy balance studies of the evolution of the Earth's core have concluded that the inner core is young, of order 1.5 Ga (Labrosse et al., 2001; Buffett, 2003; Nimmo et al., 2004) and that the inclusion of radioactive heat sources increases this age by slowing the rate of core cooling, but only by a few 100 Myrs. The presence of radioactive heat sources in the core would also provide an additional source of power for thermal convection which may help to explain how the geodynamo was sustained for times prior to the formation of the inner core.

In order to investigate the effects of inner-core growth and core internal heating on simulations of the Earth's thermal evolution, we will present three series of calculations. The A series simulations employ varying degrees of internal heating in the core and neglect the thermal effects of inner core formation. The B series simulations are identical to the A series except that the effects of inner core formation are included and core parameters are chosen so as to produce an inner core of the correct final size. Finally, two C series simulations were performed with the same core parameters as one of the B series simulations and with significantly higher initial core temperatures. In the following sections, we will describe the core and mantle models while in subsequent sections we will discuss the impact of inner core formation and core internal heating on the Earth's thermal evolution.

2. Model description

We employ a spherical axisymmetric numerical model of convection in the Earth's mantle coupled to a heat reservoir model for the core to describe the thermal evolution of the Earth. In Fig. 1(a) we show a temperature field from the end of a simulation with 4 TW of internal heating in the core along with a schematic of our core evolution model. The numerical model is set-up to be as similar as possible in thermal properties to an existing parameterized model (Butler and Peltier, 2002) which we will also explore for the sake of comparison. The effects of short time-scale and lateral temperature variations can only be investigated using the numerical model. The numerical model employed here is modified from the one described in Butler and Peltier (2000) which was itself based upon the previous version of Solheim and Peltier (1994a,b). The assumptions and governing equations of the model are briefly described in what follows.

2.1. Core model

The temperature of the core-mantle boundary, T_{cmb}, of the numerical model is assumed constant in space but is allowed to evolve in time assuming that the core is a heat reservoir from which heat flows into the mantle at a rate that depends on the temperature at the core–mantle boundary and on the evolving dynamics in the mantle. Heat energy is input to the core by the radioactive decay of ^{40}K at a rate χ_{c} and, once the inner core begins to form, by latent heating and the release of gravitational potential energy at rates χ_{l} and χ_g, respectively,

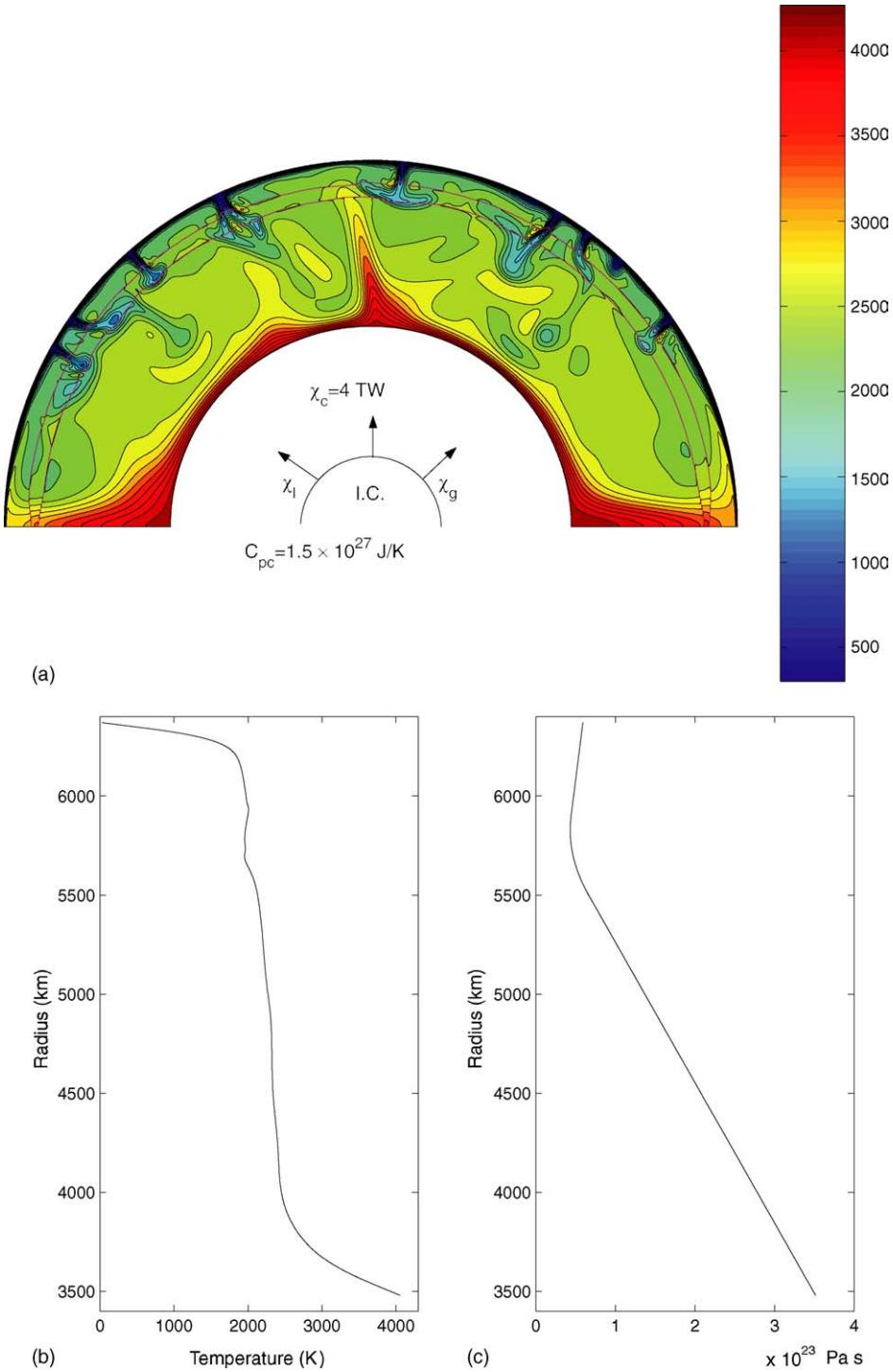

Fig. 1. (a) A contour plot of the temperature field as well as a schematic of the core model including the effects due to the growth of the inner core (I.C.). (b) The average temperature as a function of depth in the mantle and (c) the viscosity as a function of depth in the mantle at the end of a simulation B4.

so that:

$$\frac{dT_{cmb}}{dt} = \frac{2\pi k_{cmb} r_{cmb}^2}{C_{pc}} \int_0^{\pi} \left.\frac{\partial T}{\partial r}\right|_{r_{cmb}} \sin\theta \, d\theta + \frac{\chi_c + \chi_l + \chi_g}{C_{pc}}. \quad (1)$$

The quantities r_{cmb}, C_{pc}, k_{cmb} and $\left.\frac{\partial T}{\partial r}\right|_{r_{cmb}}$ represent the CMB radius, the heat capacity of the core, and the thermal conductivity and temperature gradient on the mantle side of the CMB. The latter is calculated from the evolving convection simulation. By evolving the core temperature in this manner, we are assuming that heat is transported by convection in the core much more efficiently than in the mantle and as a result, the thermal boundary layer on the mantle side of the core–mantle boundary limits heat transfer from the core to the mantle. Given the very large difference in fluid viscosity between these two regions, this assumption is entirely justified.

The quantity C_{pc} is not the true total heat capacity of the core but rather an effective heat capacity since we are multiplying it by the change in temperature at the CMB rather than the average temperature of the core. It can be calculated from

$$C_{pc} = \int_0^{r_{cmb}} \rho_{cen} \exp\left[-\frac{r^2}{L^2}\right] c_{pc} \times \exp\left[\frac{r_{cmb}^2 - r^2}{D^2}\right] r^2 \, dr. \quad (2)$$

Here r is the radius, c_{pc} is the core heat capacity per unit mass, ρ_{cen} is the density at the centre of the Earth and $\rho_{cen}\exp[-r^2/L^2]$ is a representation of the radial variation of density in the core, with the characteristic length scale L. D is a length scale characterizing the adiabatic temperature profile in the core (e.g., Labrosse et al., 2001; Buffett et al., 1996). While ρ_{cen} and L are well known from PREM, values of c_{pc} range from 860 to 670 J/kg K (Stacey, 1992; Labrosse, 2001) and D falls in the range 6000–8830 km (Labrosse et al., 2001; Labrosse, 2003), giving a range of values for C_{pc} from 1.4×10^{27} to 2.1×10^{27} J/K. We have adopted a dimensional value of 1.5×10^{27} J/K for all of the calculations shown here.

In (1), χ_c represents the rate of internal heating in the core due to the presence of ^{40}K. An upper bound of 8 TW of radioactive heating (corresponding to 1200 ppm K) in the core is obtained if it is assumed that the bulk Earth has the C1 chondrite concentration of potassium (Gessmann and Wood, 2002). In this scenario, no potassium was lost to space during the very early stages of the Earth's evolution but rather was incorporated into the core. In this study, we investigate thermal evolution models with modern-day core heating rates of 0, 1, 2, and 4 TW.

While χ_c is prescribed, we compute χ_g and χ_l using (Stacey, 1992)

$$\chi_l = 4\pi \mathcal{L} \rho_{ic} r_{ic}^2 \frac{dr_{ic}}{dt} \quad (3)$$

and

$$\chi_g = \frac{8\pi^2}{15} G \Delta\rho_{icb} \rho_c (3 r_{cmb}^2 r_{ic}^2 - 5 r_{ic}^4) \frac{dr_{ic}}{dt}. \quad (4)$$

Here r_{ic}, $\mathcal{L}$, ρ_{ic}, ρ_c, and $\Delta\rho_{icb}$ are the time-evolving radius of the inner core, the latent heat of freezing of iron at core pressures per unit mass and the mean densities of the inner-core and outer core respectively, and that part of the density jump at the inner-core boundary (ICB) that is associated with the rejection of the light element, while G represents the gravitational constant. The values of the various parameters governing the core evolution are listed in Table 1. The total latent heat, E_l, and gravitational energy, E_g released in forming an Earth-sized inner core implied by (3) and (4) are the same for all simulations and using the parameters listed in Table 1 are $E_l = 7.75 \times 10^{28}$ J and $E_g = 3 \times 10^{28}$ J. We note that the recent studies of Masters and Gubbins (2003) indicate that $\Delta\rho_{icb}$ may be as large as 620 kg/m^3 which would increase the gravitational energy release by a factor of 1.5 over the value used here. An increase of $\Delta\rho_{icb}$ by this amount would increase the predicted age of the inner core by approximately 60 Myrs. The value of the slope of the liquidus might also be slightly larger. If this value were increased to 9×10^{-9} K/Pa as suggested by Alfé et al. (2002) then the predicted age of the inner core would be increased by roughly 240 Myrs. As can be seen by inspection of (3) and (4), the rate at which this energy is released is controlled by the growth rate of the inner core. We outline below a simple model for calculating this growth rate.

Following Buffett et al. (1992), we assume a linear expansion of the liquidus temperature near the centre

Table 1
Core constants and parameters used in this study

Parameter	Symbol	Equation	Value	Units
Mean density (outer core)[a]	ρ_c	(2), (4)	1.1×10^4	$kg\,m^{-3}$
Mean density (inner core)[a]	ρ_{ic}	(3), (6)	1.27×10^4	$kg\,m^{-3}$
Density jump[b](inner/outer core)[c]	$\Delta\rho_{icb}$	(4)	400	$kg\,m^{-3}$
Radius of the outer core[a]	r_{cmb}	(1), (2), (4)	3480×10^3	m
Specific heat capacity[a]	c_{pc}	(1), (2)	675	$J\,kg^{-1}\,K^{-1}$
Latent heat[b]	$\mathcal{L}$	(3)	8.0×10^5	$J\,kg^{-1}$
Solidification temperature at the centre of the Earth[d]	$T_L(0)$	(5), (6)	5700	K
Pressure gradient for solidification temperature[b]	dT_L/dP	(5), (6)	7.33×10^{-9}	K/Pa
Liquidus parameter	Λ	(8), (9)	1.6526×10^{-10}	$K\,m^{-2}$
Thermal conductivity at the base of the mantle[e]	k_{cmb}	(1)	12	$W\,m^{-1}\,K^{-1}$

[a] Stacey (1992).
[b] Buffett et al. (1996).
[c] Due to compositional changes across inner core boundary.
[d] Anderson (2002).
[e] Osako and Ito (1991).

of the core

$$T_L(r) = T_L(0) + \frac{dT_L}{dP}(P(r) - P_0), \tag{5}$$

where P is the pressure at the radius r, $T_L(0)$ and P_0 represent the liquidus temperature and the pressure at the centre of the Earth respectively, and dT_L/dP is the pressure dependence of the liquidus temperature. If we further assume a hydrostatic variation in the pressure $P(r)$ with radius in the inner core and we approximate this relation by assuming a constant density in the inner core, we can write the following

$$T_L(r) = T_L(0) - \frac{2\pi}{3} G\rho_{ic}^2 r^2 \frac{dT_L}{dP}. \tag{6}$$

We note that the assumption of a constant density used in (6) gives an excellent representation of the radial variation of pressure from the center of the Earth to the inner core boundary, which is the only region of interest in this study. Solidification of the core material, and therefore the radius at the ICB will occur where the temperature in the core intersects the liquidus for core material. Since the outer core is thought to be convecting vigorously, the temperature profile in this region is adiabatic and the temperature at the ICB can be related to the temperature at the CMB by

$$T_L(r_{ic}(t)) = \Gamma\, T_{cmb}(t), \tag{7}$$

where $r_{ic}(t)$ represents the time-evolving radius of the inner core. The parameter Γ, which in the formulation of Labrosse et al. (2001) takes the form $\exp[(r_{cmb}^2 - r_{icb}^2)/D^2]$, depends on the thermal expansivity and heat capacity of core material as well as the acceleration due to gravity in the core. There are significant uncertainties in the values of the first two of these quantities resulting in values of Γ that lie between 1.21 and 1.64 based on the values given in Labrosse et al. (2001). Γ should also decrease as the inner core grows since the adiabatic gradient will extend over shorter distances. We ignore this last effect (which produces an error of roughly 6%) and treat Γ as a constant in each simulation. In Table 2 we list all of the simulations performed along with the final internal heating rate, the initial core temperature and the value of Γ used. For the B series of simulations, the value of Γ was chosen such that the final inner core radius in each simulation matched the present-day inner core radius of the real Earth. For simulation C0, Γ was taken to have the same value as in simulation B2 and the initial core temperature was varied until the correct-sized inner core was achieved. This simulation allows us to compare the effects of internal heating in the core with the effects of increasing the initial core temperature. Varying the initial core temperature is a significantly more computationally expensive method of achieving the correct sized inner core than varying Γ since simulations must be iterated over the entire history of the Earth, while when Γ is varied, simulations must only be iterated over the lifetime of the inner core, as we will describe below. We also performed simulation C2 with the same initial core temperature and core adiabatic gradient as simulation C0 but with 2 TW of internal

Table 2
A summary of the simulations performed

Run name	$\chi_c(t^p)$ (TW)	$T_{cmb}(t^0)$ (K)	Γ
A0	0	4300	0
A1	1	4300	0
A2	2	4300	0
A4	4	4300	0
B0	0	4300	1.556
B1	1	4300	1.46
B2	2	4300	1.3915
B4	4	4300	1.26
C0	0	5500	1.3915
C2	2	5500	1.3915
$B0_p$	0	4300	1.49
$B1_p$	1	4300	1.412
$B2_p$	2	4300	1.347
$B4_p$	4	4300	1.2465
$C0_p$	0	5500	1.3915
$C2_p$	0	5500	1.3915

We list the final core internal heating rate χ_c, the initial CMB temperature, $T_{cmb}(t^0)$ and the core adiabat parameter, Γ. A value of 0 for Γ indicates that no effects due to inner core freezing were included. A subscript p on the run name indicates a parameterized model.

heating in the core in the final state. As we will show, an inner core does not begin to form in simulation C2.

Combining Eqs. (5)–(7) we arrive at the following equation for the time-dependent radius of the inner core in terms of the temperature at the CMB

$$r_{ic}(t) = \left(\frac{T_L(0) - \Gamma\, T_{cmb}(t)}{\Lambda} \right)^{1/2}, \tag{8}$$

where we have defined the liquidus parameter

$$\Lambda = \frac{2\pi}{3} G \rho_{ic}^2 \frac{dT_L}{dP}.$$

The value of r_{ic} is updated at each time step using (8) and $dr_{ic}/dt \cong (r_{ic} - r_{ic}^-)/\Delta t$ is then calculated where r_{ic}^- is the inner core radius of the previous model time step and Δt is the model time step.

In order to choose a value of Γ such that the inner core has the correct final size as we do in the B series models, we consider (8) for the time when the inner core has just started to form and for the present-day Earth. We indicate quantities evaluated at these times with superscripts *in* and *p* respectively. For instance, the CMB temperatures at these times are T_{cmb}^{in} and T_{cmb}^{p}, and the corresponding radii are $r_{ic}^{in} = 0$ and $r_{ic}^{p} = 1221$ km. Substituting the known value of r_{ic}^{p} into (8) and solving for Γ we obtain the following result

$$\Gamma = \frac{T_L(0) - \Lambda(r_{ic}^p)^2}{T_{cmb}^p}. \tag{9}$$

The value of T_{cmb}^{p} is unknown before the start of the simulation. However, we can estimate the total change in the temperature of the core if all of the latent and gravitational energy of inner core formation were used to increase the temperature of the core. Using E_l and E_g from above, we compute $\Delta T = (E_l + E_g)/C_{pc} = 72$ K, which is much smaller than the total change in the temperature of the core during the entire 4.5 Gyr course of a simulation. As a result, the thermal effects of the solidification of the inner core can be considered to represent a perturbation to the thermal evolution of the core. This observation allows us to determine the value of the parameter Γ that is required in order to evolve an inner core of the size of the present-day Earth's. In practice, we first ran a simulation for the full age of the Earth with zero χ_l and χ_g in order to obtain a zeroth order estimate of the final temperature at the CMB, $T_{cmb}^{p,0}$. These are the A series simulations listed in Table 2. We then make the first order approximation that all of the latent heat and gravitational energy released is maintained in the core to obtain an improved estimate of the final temperature at the CMB, $T_{cmb}^{p,1} = T_{cmb}^{p,0} + \Delta T$. This estimate for $T_{cmb}^{p,1}$ is then used in (9) to obtain an estimate of the value of Γ required to grow an inner core of the same size as the one found in the real Earth. Using this value of Γ, we would then calculate T_{cmb}^{in} and by analyzing the time evolution of T_{cmb} for the first run in the absence of χ_l and χ_g, the age of the inner core was determined. The model was then rerun starting from a time just prior to the formation of the inner core using as initial conditions output from the appropriate time of the first run and including the effects of χ_l and χ_g and evolving the radius of the inner core according to (8). If the inner core were too large or too small after this second model run, we re-iterate the process for calculating Γ using an approximate final temperature at the CMB of $T_{cmb}^{p,2} + \Delta T_2$ where $T_{cmb}^{p,2}$ is the final temperature at the CMB from the new simulation and ΔT_2 is the change in the core temperature associated with melting or solidifying the extra amount of core material required to make the model inner core of the same size as the real Earth's.

By requiring the correct-sized inner core, we are emphasizing the constraints due to the total heat energy that must be transported across the core–mantle boundary over those concerning the absolute temperatures at core horizons. A similar approach was used by Labrosse et al. (2001). In order to further elucidate the energy budget in the core over the time of inner core formation, we integrate Eq. (1) over the age of the inner core which, making use of Eq. (8) and requiring that the final size of the inner core equals that of the present-day Earth, gives the following

$$\int_{t^{\mathrm{in}}}^{t^{\mathrm{p}}} Q_{\mathrm{c}}\,\mathrm{d}t = \frac{C_{\mathrm{pc}}\Lambda(r_{\mathrm{ic}}^{\mathrm{p}})^2}{\Gamma} + E_{\mathrm{g}} + E_{\mathrm{l}} + \int_{t^{\mathrm{in}}}^{t^{\mathrm{p}}} \chi_{\mathrm{c}}\,\mathrm{d}t. \tag{10}$$

Here Q_{c} is the spatially integrated heat flow at the core–mantle boundary. Eq. (10) indicates that the time required for the formation of the inner core, $t^{\mathrm{p}} - t^{\mathrm{in}}$, is equal to the time that it takes for the heat energy equal to the sum of the terms on the right-hand side to be transported by conduction across the CMB. If Q_{c} were held the same, then Eq. (10) indicates that an increase in χ_{c} would increase the age of the inner core. The first term on the right-hand side of Eq. (10) represents the energy due to the secular cooling of the core and it can be seen to decrease with increasing Γ. As can be seen from Eq. (9), the value of Γ used in our B series calculations decreases with an increasing value of the final CMB temperature which, in turn, tends to increase with increasing degrees of internal heating in the core. Physically, this means that simulations with high degrees of internal heating require us to use shallower core adiabats in order that the inner core be of the correct final size. As a result, in our formulation for the B series models, simulations with higher degrees of core internal heating must undergo increased degrees of secular cooling over the lifetime of the inner core which further increase the magnitude of the right-hand side of Eq. (10). Thus, increasing χ_{c} in our B series of runs results in two effects, both of which will increase the age of the inner core if Q_{c} is unchanged although we will show that the change in the energy of secular cooling is small compared to the direct effects of internal heating. We will also show that varying the degree of internal heating in the core will also affect the vigor of convection in the mantle which in turn will affect Q_{c}.

We could instead have chosen a fixed value of Γ for all of our simulations and initiated the growth of the inner core when the estimated temperature at the centre of the core in our model reached the liquidus temperature for core-materials for the pressure at the centre of the Earth which would result in calculations with varying final sizes of the inner core. The final size of the inner core could then be compared with that of the real Earth. This latter approach has been used in all previous investigations of inner core growth (e.g., Nimmo et al., 2004; Nakagawa and Tackley, 2004). The disadvantage of this approach, however, is that varying amounts of latent heat and gravitational energy are released. This becomes particularly important in models where large inner cores are found to grow. Also, given the existing disagreement between estimates of the required quantities (e.g., Alfé et al., 2002; Boehler, 2000) and uncertainties associated with the absolute temperature at core depths, we chose the approach described above and consider the temperature at the CMB as an output of our model to be compared with estimates of high-pressure physics analyses as we will do in the following section. We also note that all of the values for Γ in our simulations, representing the slope of the core adiabat, are within the range of experimental uncertainties. We could also have varied the values of $T_{\mathrm{L}}(0)$ and Λ within experimental uncertainties. Had a model required values of these parameters outside of the range allowed by a priori constraints, we could have rejected the model. We also note that there is a slight inconsistency in this formulation in that since we are varying Γ, we should also be varying the effective heat capacity of the core C_{pc}.

2.2. Mantle model

The mantle viscosity is assumed to vary only radially and to depend on the temperature in the mantle and hence on time. This is clearly a simplification compared with the use of a viscosity law that depends on the azimuthal angle but it allows for significant computational speed-up. Also, Brunet and Machetel (1998) compared the heat flow in calculations with laterally varying, temperature-dependent viscosity with the heat flow in simulations with only radially dependent viscosity where the radial dependence was the same as the azimuthally averaged viscosity in the temperature-dependent case and found the two to be quite similar. The radial dependence is assumed to consist of two lin-

ear segments, one in the lower mantle and one in the upper mantle and transition zone as follows:

$$\eta(r) = \frac{\eta_e - \eta_l}{r_{660} - r_{cmb}} r + \frac{\eta_l r_{660} - \eta_e r_{cmb}}{r_{660} - r_c}, \quad \text{for } r < 5500\,\text{km},$$

$$\eta(r) = \frac{\eta_u - \eta_e}{r_s - r_{660}} r + \frac{\eta_e r_s - \eta_u r_{660}}{r_s - r_{660}}, \quad \text{for } r > 5900\,\text{km}. \tag{11}$$

For the region $5500\,\text{km} < r < 5900\,\text{km}$ we use a cubic profile chosen such that the viscosity and its first derivative are continuous at $r = 5500$ km and $r = 5900$ km. The viscosity at the base of the lower mantle, η_l, at 660-km depth, η_e, and in the upper mantle, η_u, are calculated from

$$\eta_l = \eta_{l0} \exp\left[T_A\left(\frac{1}{T_L} - \frac{1}{T_{lf}}\right)\right],$$

$$\eta_e = \eta_{e0} \exp\left[2T_A\left(\frac{1}{T_u + T_L\phi_{le}} - \frac{1}{T_{uf} + T_{lf}\phi_{le}}\right)\right],$$

$$\eta_u = \eta_{u0} \exp\left[T_A\left(\frac{1}{T_u\phi_{eu}} - \frac{1}{T_{uf}}\right)\right]. \tag{12}$$

Here T_L and T_u represent the average temperature at each time step in the lower mantle, and in the transition zone and upper mantle, respectively. The values for the constants T_{uf}, T_{lf}, T_A (used to model the activation energy of material creep processes in the mantle), η_{l0}, η_{e0}, η_{u0}, ϕ_{le} and ϕ_{eu} (used to describe the adiabatic drop in temperature from the core–mantle boundary to 660 km depth and from 660 km depth to the surface) are provided in Table 3. The geotherm and radial variation in viscosity from the end of simulation B4 are shown in Fig. 1b and c respectively. The viscosity used in the model is significantly higher than values inferred on the basis of post-glacial rebound (e.g., Peltier and Jiang, 1996). As well as increasing computational efficiency, these high values are necessary so that the predicted surface heat flow is similar in magnitude to that which is observed (Butler and Peltier, 2000). The viscosity in the lower mantle is also significantly higher than the viscosity in the upper mantle and transition zone as is evidenced in Fig. 1 by the significantly larger spatial wavelength of rising plumes in the lower mantle compared with the sinking boundary layer instabilities in the upper mantle. The top and bottom boundaries, corresponding to the surface and CMB are assumed to be free-slip. It should be noted, as discussed in detail in Butler and Peltier (2000), that such model predictions of surface heat flow could be made to agree with observations for the same viscosity profile as that required to reconcile postglacial rebound data if layering were more pronounced across the 660-km horizon than that predicted by our simple representation of the endothermic phase transformation (see Solheim and Peltier, 1994a, for a discussion of the methodology currently employed in this model).

Table 3
Constants used to define the viscosity profiles in Eqs. (10) and (11).

Constant	Value	Units
T_{uf}	2099	K
T_{lf}	2931	K
T_A	55000	K
η_{l0}	2.17×10^{23}	Pa s
η_{e0}	8.52×10^{22}	Pa s
η_{u0}	4.07×10^{23}	Pa s
ϕ_{le}	0.75	Non-dim
ϕ_{eu}	0.92	Non-dim

The internal heating rate in the mantle is made time-dependent with the same intensity used in the parameterized calculations of Butler and Peltier (2002). The uranium/thorium/potassium ratios used are 1/4/10,000 following Hart and Zindler (1986) and a bulk silicate Earth uranium concentration of 21 parts per billion is assumed which gives a total modern-day heating power of 19.4 TW for the mantle and crust. We assume that 6.4 TW is stored in the continental crust and use 13 TW in our mantle model. The heat sources are fixed in position and 2 and 11 TW of heat sources are uniformly distributed in the regions above and below the 660-km depth horizon, respectively. The low heating rate in the upper mantle is used in order that the upper mantle internal heating rate matches the observed heating power in modern MORB source material.

The other thermodynamic and transport properties of the mantle are depth-dependent and are fit to be as Earth-like as possible and are described in Butler and Peltier (2000). The model also includes the effects of the phase transitions at 400 and 660-km depth with Clapeyron slopes of 3 and −2.8 MPa/K, respectively (Chopelas et al., 1994). The phase boundaries are indicated in Fig. 1 by the magenta lines and it can be seen that in places the 660-km depth phase transition is providing a partial barrier to mantle flow. The initial conditions for these calculations were taken from a pre-

vious simulation run with a similar Rayleigh number but without time varying viscosity, core–mantle boundary temperature and internal heat sources. The initial average temperature as a function of depth was chosen to lie on an adiabat with temperature at the mantle solidus for the upper mantle and the initial CMB temperature was chosen to be 4300 K for the A and B series of runs and was 5500 K for the C series. The initial CMB temperature of 4300 K was chosen based on the assumption that the initial temperature at the CMB would be the same as the liquidus temperature for lower mantle materials (Serghiou et al., 1998) and is the same initial core temperature used by Butler and Peltier (2002), Nakagawa and Tackley (2004).

3. Results

3.1. The effects of inner-core growth on thermal evolution

In Fig. 2 we show a summary of the heat flow between the various regions of the Earth for the final 2050 Myrs of the simulations without internal heating in the core. We display both the results of simulation A0 in which the effects of latent heating and gravitational energy release have been neglected (dotted-line) and the results from simulation B0 in which the inner core evolves to a final size of 1221 km (solid-line). Inner core formation begins in this model after 2744 Myrs of evolution. The advected heat flow at 660-km depth, Q_{adv}, shows the strong temporal variability associated with mantle avalanches while the conducted heat flow at 660-km depth, Q_{cond}, peaks during periods of mantle layering and drops to near zero during avalanches. One might expect that the heat flow at the core–mantle boundary, Q_{cmb}, would show the greatest change due to the thermal effects of inner core solidification; however, as can be seen, the difference in this quantity between the simulations is quite modest. The thermal effects of inner-core solidification act to perturb the time evolution of convection in the mantle, and in this case, the perturbation leads to the earlier onset of a mantle avalanche. This in turn results in the final surface heat flow, Q_s, for simulation B0 being close to 36 TW which is the observed value for the mantle contribution to this

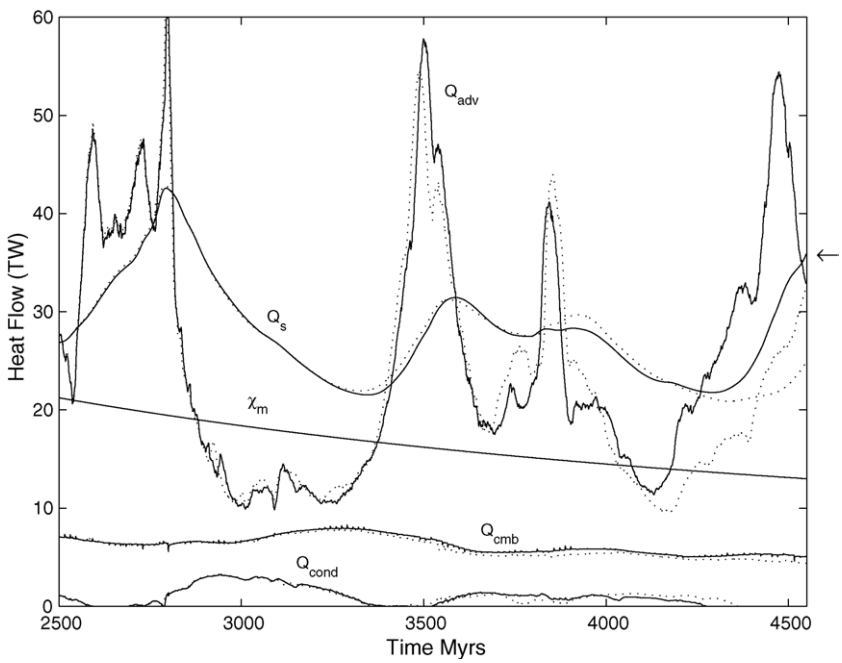

Fig. 2. The azimuthally integrated surface, Q_{s}, CMB, Q_{cmb}, internal heating rate, χ_{m}, advected heat flow at 660-km depth, Q_{adv} and conducted heat flow at 660-km depth, Q_{cond} for simulations A0 (dotted line) and B0 (solid line) Inner-core growth starts at time 2744 Myrs in simulation B0.

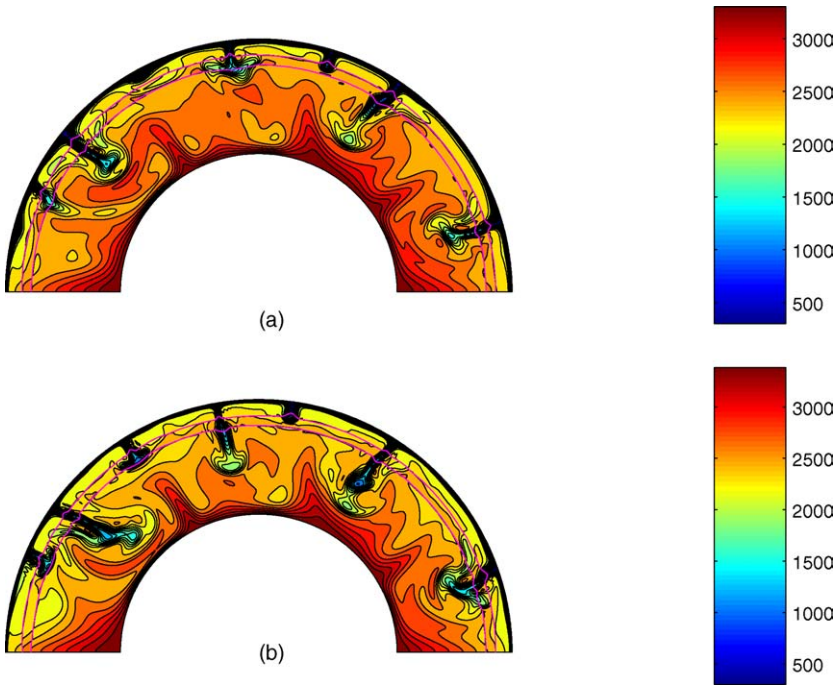

Fig. 3. The final temperature fields for calculations (a) A0 and (b) B0 with and without the effects of inner core solidification, respectively. The most significant difference is that the down-welling just to the left of the centre has broken through the 660-km depth phase transition for the latter case resulting in significantly higher heat flow due to the hot return flow that comes in contact with the top surface.

quantity (Pollack et al., 1993), indicated by the arrow on the figure, while simulation A0 has significantly too little heat flow since the mantle avalanche does not arrive before the end of the simulation. In Fig. 3a and b we display the final temperature field in the mantle for simulations A0 and B0 (note there is no internal heating in the core). Although the fields are very similar, the mantle downwelling that is located just left of the centre of the plot has broken through the 660-km phase transition in the latter case resulting in significantly higher surface heat flow for this case due to the resultant hot return flow coming in contact with the upper surface. In all of the other calculations, the effects of inner core solidification on the final surface heat flow were significantly smaller.

In Table 4 we list final state data for all of the simulations. For the sake of comparison, we include in Table 4 data calculated from the parameterized model of Butler and Peltier (2002) coupled with the same inner core model as described herein (run series with subscript p). Owing to the large temporal fluctuations, the heat flow values have been averaged over the last 800 Myrs of the simulations in order to get a characteristic final value while the temperatures represent the final values. As can be seen by comparing the results of run series A with the corresponding results of run series B, the effects of the growth of the inner core on heat flow are quite small. In all cases, the heat flow at the CMB is increased by roughly 0.5 TW while the heat flow at the surface can either be increased or decreased due to the perturbing effects of the growth of the inner core on the convective circulation in the mantle.

In Fig. 4 we display the energy budgets in the core for model B0 with no core internal heating (a) and B4 with 4 TW of core internal heating in the final state (b), for the last 2050 Myrs of the simulations (note that the vertical scale for the lower panel is twice that of the upper panel). The secular cooling of the core, χ_{sec}, is proportional to the rate of core cooling and can be calculated from $Q_{\mathrm{cmb}} - \chi_{\mathrm{c}} - \chi_g - \chi_{\mathrm{l}}$. The effects of χ_{g} and χ_{l} are relatively small and total just under 3 TW in the final state. However, unlike radioactive heat sources, their effects do not weaken with time (at least not until the core becomes completely frozen) and hence they

Table 4
The core–mantle boundary temperature, $T_{cmb}(t^p)$, and temperature drop across the core–mantle boundary $\Delta T_{cmb}(t^p)$, are the final values

Run name	Q_s (TW)	Q_c (TW)	$T_{cmb}(t^p)$ (K)	ΔT_{cmb}(K)	Urey ratio	Inner core age (Myrs)	Final I.C. radius (km)
A0	24.6	5.0	3445	514	0.58	–	–
A1	28.1	7.9	3679	798	0.51	–	–
A2	29.2	8.5	3862	937	0.49	–	–
A4	34.5	12.1	4266	1316	0.42	–	–
B0	26.07	5.43	3505	552	0.55	1756	1221
B1	27.5	8.55	3736	835	0.52	1680	1219
B2	28.58	8.91	3921	975	0.50	1647	1216
B4	34.65	12.66	4326	1354	0.41	1482	1228
C0	27.9	9.2	3923	961	0.55	1212	1207
C2	33.9	13.2	4183	1218	0.42	0	0
$B0_p$	25.5	4.93	3658	712	0.55	2075	1225
$B1_p$	27.5	7.03	3862	893	0.51	1961	1221
$B2_p$	29.72	9.27	4049	1057	0.47	1797	1221
$B4_p$	34.68	14.04	4374	1394	0.41	1451	1223
$C0_p$	30.1	8.3	3953	962	0.47	1078	1097
$C2_p$	34.5	12.3	4214	1184	0.41	0	0

The surface heat flow, Q_s, CMB heat flow, Q_c, and the Urey ratio values are the average over the last 800 Myrs of the calculation.

become increasingly significant in the energy budget of the core as time goes by. The biggest effect of these energy sources is to decrease the rate of secular cooling and hence the rate at which the temperature of the core decreases. In Fig. 5a, we show the evolution of the CMB temperature for all of the models with the same initial starting temperature of 4300 K for the case without the thermal effects of the inner core (solid line, run series A) and with it (dotted line, run series B) as well as for the parameterized model that included the

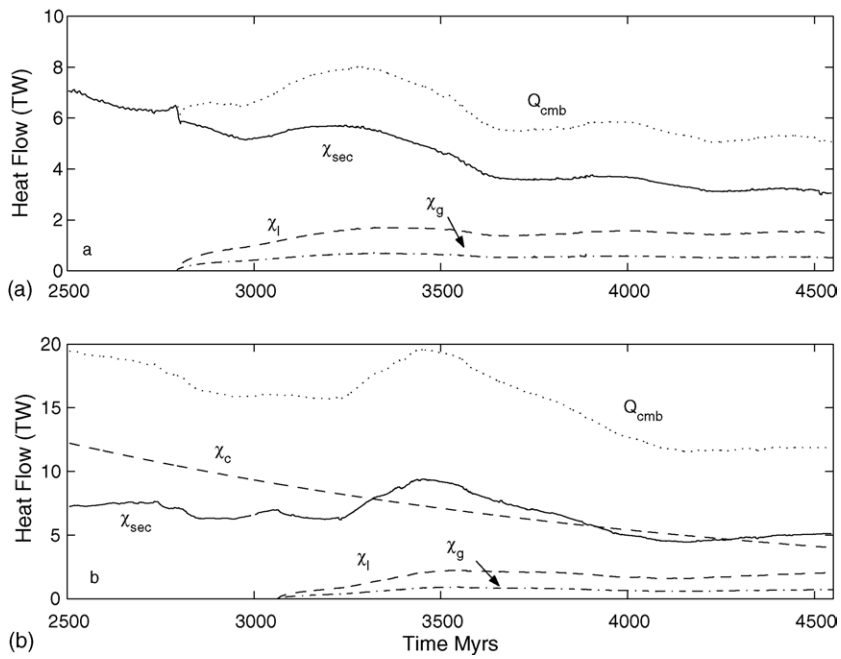

Fig. 4. The heat flow at the CMB, Q_{cmb}, internal heating rate in the core, χ_c, rate of latent heat release, χ_l, rate of gravitational energy release, χ_g and rate of secular cooling, χ_{sec}, as a function of time for the last 2050 Myrs of simulations with (a) no internal heating in the core (simulation B0), and (b) with 4 TW of internal heating in the core in the final state (simulation B4).

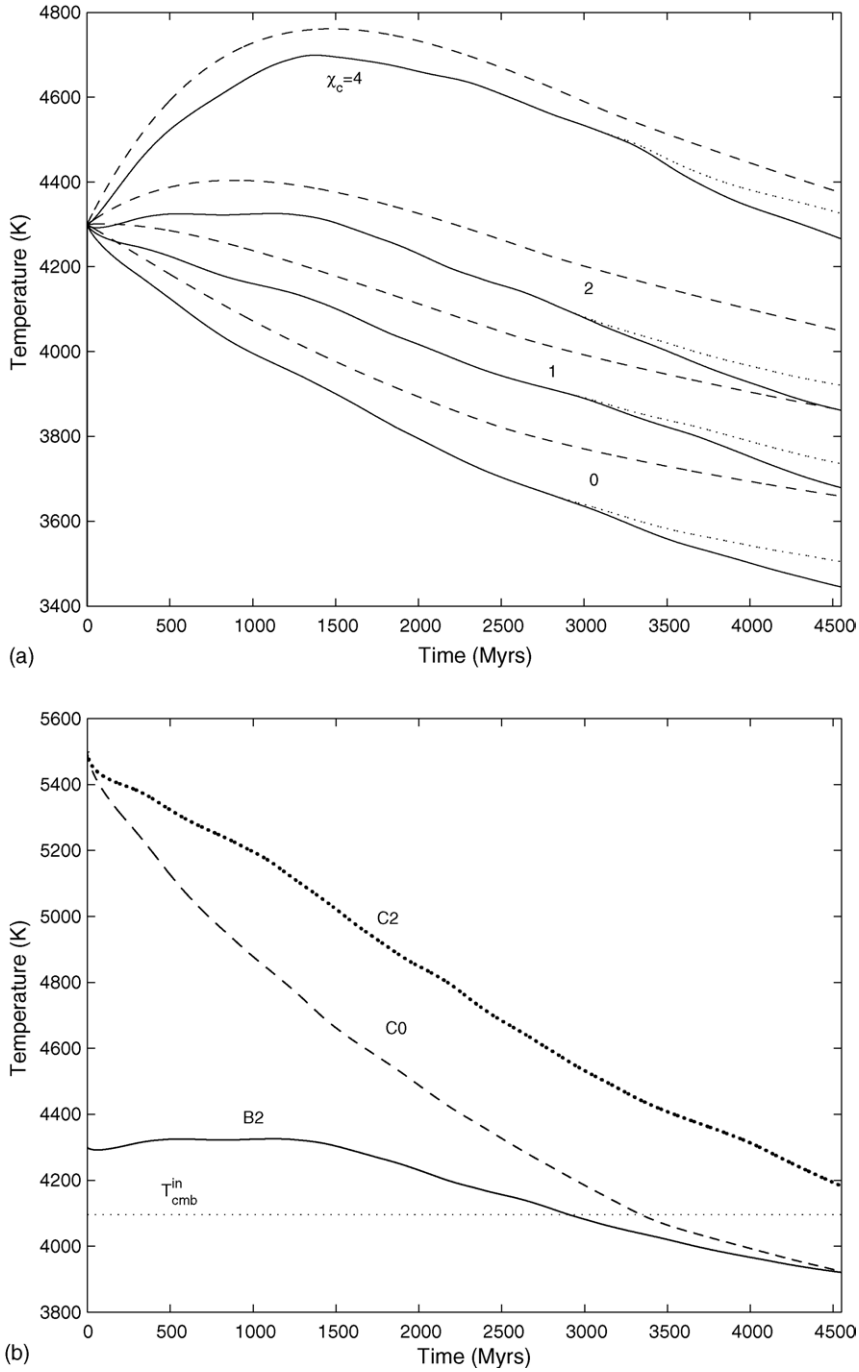

Fig. 5. (a) The evolution of T_{cmb} for models run with the final degrees of core internal heating indicated and the same initial temperature of 4300 K. Solid lines are A series models (with no effects due to inner core solidification), dotted lines are B series models (with the effects of inner core solidification) and dashed lines are the results of parameterized modeling. (b) The evolution of T_{cmb} for models B2, C0 and C2 having the same value of Γ but different degrees of internal heating and different initial core temperatures.

effects of inner-core growth (dashed-line). The slowing of the cooling of the core at the onset of inner core formation can be clearly seen. In all cases the final CMB temperature is increased by 50–60 K over its value in simulations performed excluding the thermal effects of inner core growth. These values are only slightly smaller than the value of 72 K which would result if all the heat from these sources were kept in the core, indicating that only a small fraction of the heat released due to the inner core growth has been lost to the mantle. It can also be seen that the parameterized model generally underestimates the degree of core cooling resulting in core temperatures which are roughly 100 K higher.

3.2. The effects of core potassium on inner-core growth

By inspection of Fig. 5a, it can be seen that increasing the rate of internal heating in the core increases the final core temperature if the same initial core temperature is used, as would be expected. As a result, in order to arrive at the correct-sized inner core radius using our methodology, a shallower adiabat, or lower value of Γ is used. For internal heating rates of 2 TW or greater, it can be seen that the core temperature actually increases early in Earth's history for the assumed starting temperature of 4300 K. The time of initiation of inner core growth can be discerned from the intersection of the dotted line in Fig. 5a with the solid line. The fact that the core temperature rises initially allows for the possibility that there may have initially been a solid inner core at the time of the formation of the Earth and that this core melted only to refreeze more recently, although our model does not allow for the possibility of an initial inner core. However, the calculations with 4 TW of core internal heating indicate that there would have been a significant period of 2.5 Gyrs in which there was no solid inner core in the Earth. A similar scenario is described by Buffett (2003) who considers the possibility that there may have been an initial inner core that melted at least partially before it began to refreeze.

In Fig. 5b we plot the time evolution of the CMB temperature for simulations B2, C0 and C2. Simulations B2 and C0 employ the same value of Γ but the former has 2 TW of internal heating in the final state and an initial temperature of 4300 K while the latter has no internal heating in the core and an initial temperature of 5500 K. The final temperatures are essentially the same for these two runs by design, since they must be if the inner-cores in the two simulations are to have the same radii using the same value of Γ. It can be seen that, especially early on, the temperature decreases much more rapidly for the simulation with the hotter initial core temperature since there is a greater temperature difference between the core and the mantle and since there is no source of heat in the core to buffer the CMB cooling. We also indicate the temperature at which the inner core begins to freeze, $T^{\mathrm{in}}_{\mathrm{cmb}}$, and it can be seen by the time when the CMB temperature curves intersect this line (and from the data in Table 4) that the age of the inner core is reduced for this latter case by 426 Myrs. From the data in Table 4, it can also be seen that the heat flow at the CMB averaged over the final 800 Myrs is very similar for these two calculations and as a result, the difference in the cooling rate for the final stages of these two simulations is mostly due to the difference in the core internal heating rate. In Table 5 we list the

Table 5
Summary of the energy budget of the core over the lifetime of the inner core for the simulations indicated

Run name	$T^{\mathrm{in}}_{\mathrm{cmb}} - T^{\mathrm{p,f}}_{\mathrm{cmb}}$ (K)	E_{sec} (10^{28} J)	E_{g} (10^{28} J)	E_{l} (10^{28} J)	$\int_{t^{\mathrm{in}}}^{t^{\mathrm{p}}} \chi_{\mathrm{c}}(t)\,\mathrm{d}t$ (10^{28} J)	$\int_{t^{\mathrm{in}}}^{t^{\mathrm{p}}} Q_{\mathrm{c}}\,\mathrm{d}t$ (10^{28} J)	Inner core age (Myrs)
B0	158	23.7	2.99	7.75	0	34.4	1756
B1	168	25.2	2.97	7.71	8.7	44.5	1680
B2	175	26.3	2.95	7.65	16.8	53.7	1647
B4	198	29.7	3.03	7.88	28.8	69.4	1482
C0	173	25.9	2.89	7.48	0	36.3	1212

$T^{\mathrm{in}}_{\mathrm{cmb}} - T^{\mathrm{p,f}}_{\mathrm{cmb}}$ is the temperature change at the CMB over the lifetime of the inner core, E_{sec} is the energy change due to the secular cooling of the core, E_{g} and E_{l} are the gravitational energy and latent heat released due to inner core freezing, $\int_{t_i}^{t_{\mathrm{p}}} \chi_{\mathrm{c}}(t)\mathrm{d}t$ is the total energy due to internal heating over the lifetime of the core while $\int_{t_i}^{t_{\mathrm{p}}} Q_{\mathrm{c}}\mathrm{d}t$ is the total heat energy flux across the CMB.

values of the various terms on the right-hand side of Eq. (10). The secular cooling term, E_{sec}, as well as the terms describing the release of latent heat and gravitational potential energy are essentially the same for these two simulations with the small differences being due to the small differences in the final inner core radii. The only significantly different term is the energy released by internal heating in the core which increases the calculated age of the inner core.

Also plotted in Fig. 5b is the evolution of the temperature at the CMB for calculation C2 which employs the same initial core temperature and core adiabatic gradient as simulation C0 but includes 2 TW of internal heating in the final state. This calculation was not constrained to evolve an Earth-like inner core and as can be seen by the fact that the CMB temperature never cools below T^{in}_{cmb} that an inner core never even begins to form in this model. It can also be seen that for simulation C2, the core does not show an early warming phase as it does in simulation B2 with a cooler initial core temperature and the same degree of internal heating in the core.

In Fig. 6 we plot the radii of the inner cores for all of the B series simulations and simulation C0 as a function of time. For the B series simulations, which employ the same initial core temperature, the onset of inner core growth is delayed slightly for calculations with higher degrees of internal heating in the core; however, the inner core grows faster in these calculations and all models reach the present day with essentially the same inner-core radius due to the methodology described in Section 2. The changes in the curvature seen in these plots correspond to fluctuations in CMB heat flow due to variations in the convective flow in the mantle. The predicted age of the inner core in all of our models is between 1.2 and 1.8 Ga, similar to the results of Labrosse et al. (2001), Nimmo et al. (2004). Although the final core temperature is higher in calculations with more internal heating, as can be seen in Fig. 5a, the temperature is decreasing at a greater rate which results in a relatively recent time for the formation of the inner core given the formulation of the B series models. Due to the short-timescale fluctuations in the numerical model, this trend is more apparent in the parameterized convection calculations, but it is evident in the results of both models. The greater rate of decrease in the core temperature in the cases with high internal heating rate is a result of the fact that the lower-mantle temperature

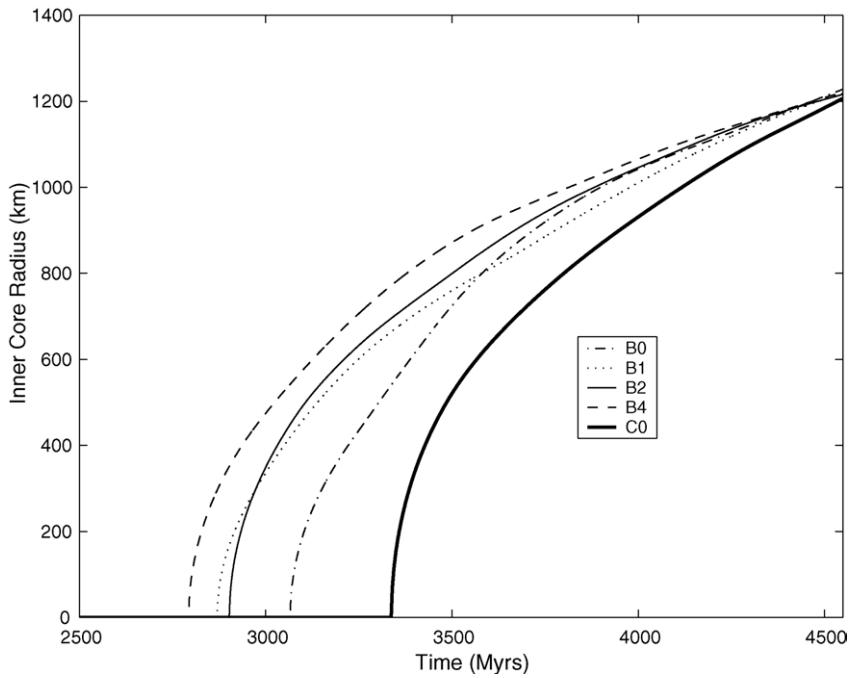

Fig. 6. The radius of the inner core as a function of time for calculations with variable degrees of internal heating in the core.

is increased due to its contact with the hot core. These high temperatures in the lower mantle in turn result in lower lower-mantle viscosity, which in turn results in more rapid convection and a more rapid decrease in the temperature of the core. As we show in Table 4, the final temperature jump across the thermal boundary layer at the base of the mantle also increases with the degree of core internal heating which also results in more rapid core cooling. The relatively short half-life of the ^{40}K isotope results in a great deal of heating in the core early in Earth's history but relatively little remains to buffer the core temperature in the latter part of the calculation. As can be seen from the data in Table 5, the total heat energy that must be transported across the CMB is significantly increased by the presence of strong internal heating in the core, mostly due to the internal heating itself, with a small effect due to the increase in the magnitude of the secular cooling term resulting from the use of a shallower adiabat in strongly internally heated calculations. The increase in the CMB heat flow overwhelms these effects, however, and as a result, models that start with the same initial core temperature and require an Earth-like final inner core size (run series B) show a slight decrease in the age of the inner core with increasing core internal heating rate.

Simulation C0, with no internal heating in the core and a much higher initial core temperature, has by far the greatest inner core growth rate and hence the youngest inner core. This is due to the relatively high core temperature near the end of simulation C0 that results in high CMB heat flow and the absence of internal heating in the core to buffer the decrease in the core temperature. It is interesting to compare the results of this simulation with simulation B0 since both of these simulations require essentially the same integrated heat transport across the CMB in order to form an Earth-like inner core (see the data in Table 5). As can be seen from the data in Table 4, the final CMB temperature is much higher for case C0 which results in much higher CMB heat flow which, in turn, results in the formation of an Earth-like inner core in a shorter period of time.

3.3. The effects of core potassium on the earth's thermal evolution

In Fig. 7 we show the time evolution of the heat flow between the various regions in the Earth as well as the heat generated by radioactive sources in the mantle and core for calculation B4 and for the corresponding parameterized simulation, $B4_p$. It can be seen that the parameterized model would be in reasonable agreement with the numerical model if the latter were smoothed on a time scale of roughly 500 Myrs. For this calculation, the final surface heat flow (Fig. 7a dotted line) is significantly less than the modern-day observed value (indicated by the arrow on the graph). It can also be seen that the final state of the mantle is one of strong layering, as evidenced by the low advected heat flow at 660 km depth (Fig. 7a, solid line). The exact timing of periods of high and low mantle surface heat flow, which in this model are controlled largely by the flux of mass across the 660-km phase transition, are the result of the properties of the mantle convection model but also of the initial azimuthal temperature distribution and hence are somewhat arbitrary. As we demonstrated in Section 3.1, a small perturbation could cause a significant difference in the final surface heat flow that the model delivers. As might be expected, the data in Table 4 indicate that the time-averaged final surface heat flow increases with the degree of internal heating in the core. An Earth-like final surface heat flow is achieved for simulation B4 with a core internal heating rate of 4 TW, in general agreement with the parameterized convection results of Breuer and Spohn (1993). Simulation C2 with an elevated initial core temperature and 2 TW of internal heating in the core also delivers close to the observed value for the Earth. Given the strong temporal variability of the surface heat flow in these calculations, the possibility exists that there could be less internal heating in the core provided that the modern-day Earth is in a time of relatively vigorous convection and high heat flow. Also shown in Table 4 are the Urey ratios (defined as the ratio of the internal heating rate in the mantle to the surface heat flow) for each simulation averaged over the last 800 Myrs. It can be seen that these quantities decrease systematically with the internal heating rate in the core for models with the same initial core temperature. Simulation C0 has a mean final surface heat flow that is greater than B1 but less than B2. In Table 6 we display the energy budget for the core over the lifetime of the Earth for the B and C series models. It can be seen that simulations C0 and C2 have significantly greater degrees of core secular cooling since they had a significantly hotter start. In simulation C0, the total heat flux across

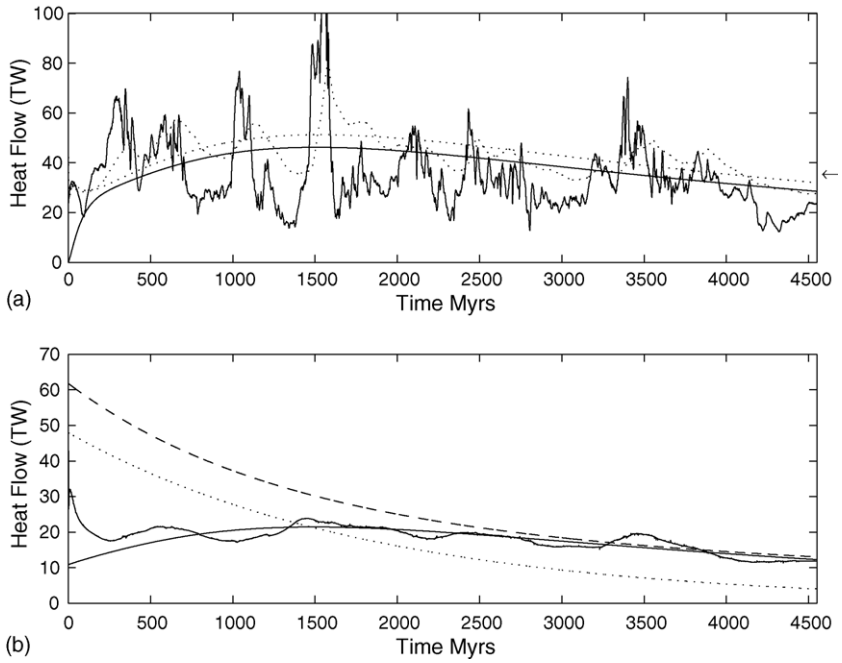

Fig. 7. Summary of heat flows as a function of time for simulations B4 (rapidly varying lines) and $B4_p$ (smooth lines). (a) The advected heat flow at 660-km depth (solid line) and the surface heat flow (dotted line). The observed final heat flow in the Earth is indicated by the arrow. (b) The heat flow at the core–mantle boundary (solid lines) and the internal heating rate in the mantle (dashed line) and core (dotted line).

the CMB is only slightly less than that of simulation B4 and is considerably greater than the rest of the B series simulations. Unlike simulation B4, however, this heat flux was concentrated near the beginning of the simulation and resulted in higher surface heat fluxes at that time whereas the slow release of heat in the core in simulation B4 caused higher surface heat flows at later times. As a result, increasing the initial core temperature is a less efficient mechanism for increasing the final surface heat flow than is internal heating.

The heat flow from the core into the mantle is also shown in Fig. 7b (solid line) and the average over the last 800 Myrs of the various simulations is also displayed in Table 4. As would be expected, this quantity also increases with increasing internal heating in the core. Recent estimates of the heat flow at the core–mantle boundary which included the heat flow due to large scale convection as well as that carried by isolated plumes, obtained values of 6–8 TW (Anderson, 2002), while Buffett (2002) estimates values of 6–12 TW based on the temperature drop across the core mantle boundary as well as the thermal boundary layer thickness and the thermal conductivity of lower mantle materials. The results of our calculations are all close to falling within the latter range for the estimate of this quantity. A value of 6 TW has recently been estimated by Nimmo et al. (2004) for the heat flow conducted down the core adiabat and is a lower bound on the CMB heat flow required to sustain the geodynamo prior to the formation of the inner core. All of our models meet this

Table 6
Summary of the energy budget of the core over the entire length of the simulations

Run name	$E_{sec}(10^{28}$ J)	$\int_{t^0}^{t^p} \chi_c(t)\,dt(10^{28}$ J)	$\int_{t^0}^{t^p} Q_c\,dt\ (10^{28}$ J)
B0	119	0	130
B1	84.6	63.4	158
B2	56.8	127	194
B4	−3.9	253	260
C0	236	0	247
C2	197.5	127	324

E_{sec} is the energy change due to the secular cooling of the core, $\int_{t^0}^{t_p} \chi_c(t)\,dt$ is the total energy due to internal heating over the lifetime of the Earth while $\int_{t^0}^{t_p} Q_c\,dt$ is the total heat energy flux across the CMB over the lifetime of the Earth.

criterion; however, the strongly internally heated models and models with elevated initial core temperatures have significantly higher CMB heat flow particularly at early times and hence, the operation of a geodynamo early in the history of the Earth is more plausible for these cases. Simulations B2 and C0 have very similar final values of Q_c indicating that this quantity is mostly controlled by the temperature at the CMB in these models.

Estimates of the temperature at the CMB from high pressure physics range from 4161 K (Alfé et al., 2002) to 3650 K (Anderson, 2002). Comparing these values with those from our simulations shown in Table 4, it can be seen that the final core temperatures obtained in models B0 and B4 are somewhat too low and too high, respectively, while models B1, B2, C0 and C2 have final CMB temperatures that are at least close to falling within this range. Clearly, there is a trade-off between the initial core temperature and internal heating rate in the core and simulations C0 and B2 were designed so as to finish with the same CMB temperature. It should also be noted that the CMB temperature for simulation B4 is higher than the estimated solidus temperature of 4300 K for mantle materials at CMB pressures (Serghiou et al., 1998) indicating that partial melting would be taking place in the D'' layer. Although partial melting in D'' may explain the seismically observed ultra-low velocity zones, (Williams and Garnero, 1996), mantle plumes that rise from the CMB will also preserve the potential temperature of the CMB. Since the mantle solidus temperature decreases with height faster than the adiabat (e.g., Serghiou et al., 1998), one would then expect partial melting in up-welling mantle plumes throughout the lower mantle.

Anderson (2002) also estimated the temperature drop across the thermal boundary layer at the base of the mantle to be 1200 K, which is slightly larger than the value of Boehler (2000) of 1000 K. In Table 4, we list the final value of the temperature drop across the thermal boundary layer at the base of the mantle for each of the simulations (ΔT_{cmb}). It can be seen that this quantity increases significantly with the degree of core internal heating and that only simulations with at least 2 TW of core internal heating or that have a high initial core temperature have temperature drops that are sufficiently large, while calculation B4 has a temperature drop that is slightly too large.

4. Discussion and conclusions

We have described a set of simulations of the Earth's thermal history using a numerical model of convection in the mantle. In most cases, we have required that our simulations produce an inner core that has the same radius as that of the real Earth. For models with the same initial temperature, we have accomplished this by varying the assumed value of the adiabatic temperature gradient in the core. A further simulation was performed in which we varied the initial core temperature using a fixed value for the adiabatic gradient. The requirement that each simulation delivers the correct value for the final inner core radius results in there always being very similar amounts of energy released due to inner-core solidification. As estimates of the thermal parameters characterizing the core improve, we may be able to further restrict this class of models. However, our results point to the need for caution in using the final size of the inner core in a thermal evolution model as a test of the success or failure of a given model given the relatively wide range of models that we have found capable of evolving so as to deliver the correct final radius of the inner-core. The effects of latent heating and gravitational energy release were found to become significant in the later stages of core evolution and in all cases were found to increase the temperature at the CMB by 50–60 K. We have also shown that the effects of latent heating and gravitational energy release can perturb convection in the mantle leading to a variation in the timing of major mass flux events which can in turn significantly affect the calculated surface heat flow.

In agreement with previous analyses, we estimate an age of the inner core that is close to 1.5 Gyrs. In all cases the effect of core internal heat sources on the age of the inner core is found to be relatively small. Comparing models B2 and C0 that obtained the same final core temperature but had different initial core temperatures and different degrees of core internal heating, we found that including internal heat sources in the core in the form of radioactive potassium increased the age of the inner core. The heat flows at the CMB near the end of these simulations were very similar, as can be seen in Table 4, and the effect of core internal heating was to slow the rate of core cooling and inner core growth. This model comparison is probably the most directly comparable to the energy balance calculations of Labrosse et al. (2001) who also required their mod-

els to deliver the correct final radius for the inner core and who showed a modest increase in the age of the inner core with increasing degrees of internal heating. In contrast, in comparing our model calculations that require the same initial core temperature and the same final inner-core radius, we find that the age of the inner core actually decreases somewhat in the presence of core radioactive heating due to increased temperatures at the CMB which in turn lower the viscosity in the lower mantle which result in increased CMB heat flows.

Unlike most parameterized convection studies, our numerical model shows large short-time scale fluctuations in the surface heat flow. Grigné et al. (2005) introduced the effects of varying the aspect ratio of convective rolls into parameterized convection models in order to mimic the effects of Wilson cycles and they showed that there can be significant variation in the calculated surface heat flow on time scales of order 100 Myrs. They also concluded that one solution to the "Urey ratio paradox" is that the observed modern-day surface heat flow is unusually high. If the surface heat flow observed today does not reflect a mantle that is in an unusually active state such as an avalanche (e.g., Solheim and Peltier, 1994a,b), then our analyses indicate that a model with a modern-day core internal heating rate of roughly 4 TW best fits the surface heat flow constraint. Increasing the initial temperature of the core is another mechanism for increasing the final surface heat flow and our model with a hot initial CMB temperature of 5500 K and 2 TW of internal heating in the final state also delivers an Earth-like surface heat flow. A model with 4 TW of core internal heating leads to a temperature at the CMB that is somewhat too high, however. Preliminary investigations using the parameterized model alone have indicated that it is possible to still maintain the correct surface heat flow in a model with 4 TW in the core in the final state and have an appropriate CMB temperature if lower mantle viscosities are used since more efficient convection in the mantle decreases the build up of heat in the core that occurs in the strongly heated core simulations. Thermal history scenarios with lower degrees of internal heating in the core and active present-day mantle avalanches remain strong possibilities, however.

Investigations with lower absolute mantle viscosities would also be of interest since they would be employing higher effective Rayleigh numbers which would result in higher degrees of mantle layering induced by the 660-km depth endothermic phase transition (e.g. Butler and Peltier, 2000). At such high Rayleigh numbers, a net decrease in the degree of mantle layering over the course of a simulation due to the decreasing effective Rayleigh with time might occur and simulations might display the surface heat flow buffering effects of Rayleigh number dependent layering seen in Butler and Peltier (2002). This effect was shown in the context of parameterized models to allow for simulations that solved the 'Urey ratio paradox' without the need for internal heat sources in the core.

Further investigations are clearly needed to investigate effects such as different mantle viscosity profiles and the effects of laterally varying temperature-dependent viscosity. One effect of temperature-dependent viscosity would be the creation of a low viscosity layer at the base of the mantle which would affect the type of plumes formed and their morphology (e.g., Jellinek and Manga, 2004). The results of Labrosse (2002), however, indicate that the main mode of heat transfer at the CMB is the conductive heating of cold downwellings so this effect should not significantly affect our conclusions concerning heat transport at this horizon. Also of interest would be the inclusion of a better representation of surface plates. Our use of a free-slip surface boundary condition without a large viscosity increase in the lithosphere likely results in our over-estimating the surface heat flow, and hence the rate of mantle cooling, somewhat. In particular, the results of Lowman et al. (2001) indicate that surface heat flow is reduced in simulations when plates with large aspect ratios are imposed. Including the insulating effects of continents would be expected to decrease the surface heat flow. However, the recent results of Lenardic et al. (2005) indicate that the presence of continents may actually increase the surface heat flow since the mantle would be made warmer and hence the viscosity would be reduced. This is quite similar to the effect that we have reported herein, that for models with the same initial temperature, the addition of internal heating in the core actually decreases the predicted age of the inner core due to warmer temperatures at the CMB and the resulting decrease in mantle viscosity and increased heat flow. It would also be interesting to compare the results obtained in spherical axisymmetric geometry with results calculated in a full three dimensional sphere. Machetel et al. (1995) com-

pared the predictions of models calculated in spherical axisymmetric geometry with those calculated in a full three dimensional sphere for various geophysical observables and found the two types of models to be in reasonable agreement. Simulating convection over the age of the Earth and exploring the effects of varying parameters in three dimensional spherical geometry remains a computationally prohibitive task. In so far as the investigation of dynamical influences upon the thermal history of the planet is concerned, it will therefore appear that the axisymmetric spherical model that we have developed will continue to be extremely useful.

Acknowledgements

We would like to acknowledge the helpful reviews by Francis Nimmo and an anonymous referee whose comments significantly improved this manuscript.

References

Alfé, D., Gillan, M.J., Price, G.D., 2002. Composition and temperature of the Earth's core constrained by combining ab initio calculations and seismic data. Earth Planet Sci. Lett. 195, 91–98.

Anderson, O.L., 2002. The power balance at the core–mantle boundary. Phys. Earth Planet Int. 131, 1–17.

Arkani-Hamed, J., Toksöz, M.N., Hsui, A.T., 1981. Thermal evolution of the Earth. Tectonophysics 75, 19–30.

Boehler, R., 2000. High-pressure experiments and the phase diagram of mantle and core materials. Rev. Geophys. 38, 221–245.

Brandon, A.D., Walker, R.J., Puchtel, I.S., Becker, H., Humayun, M., Revillon, S., 2003. Os-186–Os-187 systematics of Gorgona Island komatiites: implications for early growth of the inner core. Earth Planet Sci. Lett. 206, 411–426.

Breuer, D., Spohn, T., 1993. Cooling of the Earth. Urey ratios, and the problem of potassium in the core. Geophys. Res. Lett. 20, 1655–1658.

Brunet, D., Machetel, P., 1998. Large-scale tectonic features induced by mantle avalanches with phase, temperature, and pressure lateral variations in viscosity. J. Geophys. Res. 103, 4929–4945.

Buffett, B.A., 2003. The thermal state of Earth's core. Science 299, 1675–1677.

Buffett, B.A., 2002. Estimates of heat flow in the deep mantle based on the power requirements for the geodynamo. Geophys. Res. Lett., 29, Art.No. 1566.

Buffett, B.A., Huppert, H.E., Lister, J.R., 1996. On thermal evolution of the Earth's core. J. Geophys. Res 101, 7989–8006.

Buffett, B.A., Huppert, H.E., Lister, J.R., 1992. Analytical model for solidification of the Earth's core. Nature 356, 329–331.

Butler, S.L., Peltier, W.R., 2002. Thermal evolution of Earth: models with time-dependent layering of mantle convection which satisfy the Urey ratio constraint. J. Geophys. Res 107 (B6), 3.

Butler, S.L., Peltier, W.R., 2000. On scaling relations in time-dependent mantle convection and the heat transfer constraint on layering. J. Geophys. Res 105, 3175–3208.

Chabot, N.L., Drake, M.J., 1999. Potassium solubility in metal: the effects of composition at 15 kbar and 1900 C on partitioning between iron alloys and silicate melts. Earth Planet Sci. Lett. 172, 323–335.

Chopelas, A., Boehler, R., Lo, T., 1994. Thermodynamics and behaviour of Mg_2SiO_4 at high pressure: implications for γ-Mg_2SiO_4 phase equilibrium. Phys. Chem. Miner. 21, 351–359.

Davies, G.F., 1980. Thermal histories of convective Earth models and constraints on radiogenic heat production in the Earth. J. Geophys. Res 85, 2517–2530.

Gessmann, C.K., Wood, B.J., 2002. Potassium in the Earth's core?. Earth Planet Sci. Lett. 200, 63–78.

Grigné, C., Labrosse, S., Tackley, P.J., 2005. Convective heat transfer as a function of wavelength: implications for the cooling of the Earth. J. Geophys. Res. 110, B03409 doi:10.1029/2004JB003376.

Hart, S., Zindler, A., 1986. In search of a bulk-earth composition. Chem. Geol. 57, 247–267.

Honda, S., Iwase, Y., 1996. Comparison of the dynamic and parameterized models of mantle convection including core cooling. Earth Planet Sci. Lett. 131, 133–145.

Ito, E., Morooka, K., Ujike, O., 1993. Dissolution of K in molten iron at high temperature and pressure. Geophys. Res. Lett. 20, 1651–1654.

Jellinek, A.M., Manga, M., 2004. Links between long-lived hot spots, mantle plumes, D″, and plate tectonics. Rev. Geophys. 42, RG3002.

Labrosse, S., Poirier, J.-P., Le Mouël, J.-L., 2001. The age of the inner core. Earth Planet Sci. Lett. 190, 111–123.

Labrosse, S., 2002. Hotspots, mantle plumes and core heat loss. Earth Planet Sci. Lett. 199, 147–156.

Labrosse, S., 2003. Thermal and magnetic evolution of the Earth's core. Phys. Earth Planet Int. 140, 127–143.

Lassiter, J., 2004. Role of recycled oceanic crust in the potassium and argon budget of the Earth: toward a resolution of the "missing argon" problem. Geochem. Geophys. Geosys. 5, Q11012 doi:10.1029/2004GC000711.

Lee, K., Jeanloz, R., 2003. High-pressure alloying of potassium and iron: radioactivity in the Earth's core?. Geophys. Res. Lett. 30 (23).

Lenardic, A., Moresi, L.N., Jellinek, A.M., Manga, M., 2005. Continental insulation, mantle cooling, and the surface area of oceans and continents. Earth Planet. Sci. Lett. 234, 317–333.

Lowman, J.P., King, S.D., Gable, C.W., 2001. The influence of tectonic plates on mantle convection patterns, temperature and heat flow. Geophys. J. Int. 146, 619–636.

Machetel, P., Thoroval, C., Brunet, D., 1995. Spectral and geophysical consequences of 3-D spherical mantle convection with an

endothermic phase change at 670 km discontinuity. Phys. Earth. Planet Int. 88, 43–51.
Masters, T.G., Gubbins, D., 2003. On the resolution of density within the Earth. Phys. Earth Planet Int. 140, 159–167.
McDonough, W.F., Sun, S.-s., 1995. The composition of the Earth. Chem. Geol. 120, 223–253.
McDonough, W.F., 2004. Compositional model for the Earth's core. In: Carlson, R.W., Holland, H.D., Turekian, K.K. (Eds.), Treatise on Geochemistry: The Mantle and Core, vol. 2. Elsevier, Oxford 547–569.
Mollett, S., 1984. Thermal and magnetic constraints on the cooling of the Earth. Geophys. J. R. Astro. Soc. 76, 653–666.
Murthy, V.M., van Westrenen, W., Fei, Y.W., 2003. Experimental evidence that potassium is a substantial radioactive heat source in planetary cores. Nature 423, 163–165.
Nakagawa, T., Tackley, P.J., 2004. Effects of thermo-chemical mantle convection on the thermal evolution of the Earth's core. Earth Planet Sci. Lett. 220, 107–119.
Nimmo, F., Price, G.D., Brodholt, J., Gubbins, D., 2004. The influence of potassium on core and geodynamo evolution. Geophys. J. Int. 156, 363–376.
Osako, M., Ito, E., 1991. Thermal diffusivity of $MgSiO_3$ perovskite. Geophys. Res. Lett. 18, 239–242.
Peltier, W.R., Jiang, X., 1996. Mantle viscosity from the simultaneous inversion of multiple data sets pertaining to postglacial rebound. Geophys. Res. Lett. 23, 503–506.
Pollack, H.N., Hunter, S.J., Johnson, J.R., 1993. Heat flow from the Earth's interior: analysis of the global data set. Rev. Geophys. 31, 267–280.
Schubert, G., Stevenson, D., Cassen, P., 1980. Whole planet cooling and the radiogenic heat source content of the Earth and Moon. J. Geophys. Res 85, 2531–2538.
Serghiou, G., Zerr, A., Boehler, R., 1998. $(Mg,Fe)SiO_3$-perovskite stability under lower mantle conditions. Science 280, 2093–2095.
Sherman, D.M., 1990. Chemical bonding and the incorporation of potassium into the Earth's core. Geophys. Res. Lett. 17, 693–696.
Sharpe, H., Peltier, W.R., 1978. Parameterized mantle convection and the Earth's thermal history. Geophys. Res. Lett. 5, 737–740.
Solheim, L., Peltier, W.R., 1994. Avalanche effects in phase transition modulated thermal convection: a model of the Earth's mantle. J. Geophys. Res 99, 6997–7018.
Solheim, L., Peltier, W.R., 1994. Phase boundary deflections at 660 km depth and episodically layered isochemical convection in the mantle. J. Geophys. Res. 99, 15861–15875.
Stacey, F.D., Stacey, C.H.B., 1999. Gravitational energy of core evolution: implications for thermal history and geodynamo power. Phys. Earth Planet Int. 110, 83–93.
Stacey, F.D., 1992. Physics of the Earth, 3rd ed. Brookfield Press, Brisbane, Australia.
Williams, Q., Garnero, E.J., 1996. Seismic evidence for partial melt at the base of Earth's mantle. Science 253, 1528–1530.
Yuen, D.A., Balachandar, S., Steinbach, V.C., Honda, S., Reuteler, D.M., Smedsmo, J.J., Lauer, G.S., 1995. Non-equilibrium effects of core cooling and time-dependent internal heating on mantle flush events. Nonlinear Process. Geophys. 2, 206–221.